Removal of Foggy Noise in An Image

K.Hema Maline[1], G.Aparanjita[2], D.Srilalitha[3], CH.L.V.D.V.Prasad[4], M.T.S.Chandu[5]
SWARNANDHRA COLLEGE OF ENGINEERING AND TECHNOLOGY, NARASAPUR

Abstract- Outdoor images may cause limited visibility and low contrast due to haze noise. That haze noise is removed based on the estimate airlighting. Contrast and colour of the captured pictures are degraded under foggy weather conditions and this degradation is often attributed to estimate airlight. In this case, haze limits visibility and reduces image contrast in outdoor images. The degeneration is different for every pixel and depends on the distance of the scene point from the camera. This dependency is expressed in the transmission coefficients. Existing methods solve the single image dehazing problem using various patch-based priors. Compared to previous work, we propose an efficient algorithm that is linear in size and shape of the image. In this, First we are taking the image as per the commands, using the technique as local data set. So, we are clustering the RGB pixel values of each image, using K-means of a maximum of nearly 1000 clusters. Due tohaze, small particles in the air that scatter the light in the atmosphere so, the outdoor images often suffer from low contrast and limited visibility So that, the problem was cleared by using function as estimate airlighting. In this airlighting, several types of sub functions are used to remove unwanted noise in outdoor images and gives clear visibility of an image.

I. INTRODUCTION

In this, Outdoor images often suffer from low contrast and finite visibility due to haze, tiny particles in the air that disperse the light in the atmosphere. Haze is independent of scene brightness and has two effects on the captured image. It decreased the signal of the watched location, and it found an extra part to the image, termed the position light, or airlight. The image degeneration caused by haze increases with the distance from the camera, since the scene radiance decreases and the airlight magnitude increases. Thus, hazy images can be modelled as a per-pixel convex combination of a haze-free image and the global airlight. Our goal is to recover the RGB values of the haze-free image and the transmission for each pixel. This is an ill posed problem that has an underdetermined system of three equations and

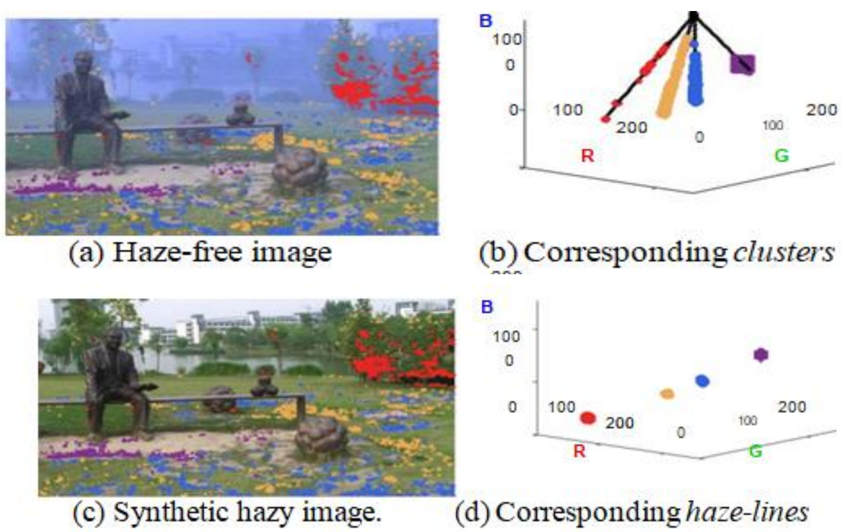

Fig.1: Non-Local Image Dehazing. (a) Pixels of a haze free colour image are clustered using K-means. Pixels belonging to four of the clusters are marked. Note that the pixels are non-local and are spread all over the image plane. (b) The four colour clusters are depicted in RGB space. Colours of the clusters correspond to the highlighted pixels in (a). (c) Synthetic haze is added to (a). The same clustered pixels are marked, but their observed colours are affected by different amounts of haze. (d) The hazy pixels depicted in RGB colour space. They are distributed along lines, termed haze-lines, passing through the airlight, marked in black. Here, we use the observation that colours of a haze-free image can be well approximated by a few hundred distinct colours [14]. This implies that pixels in a hazy image can be modelled by lines in RGB space that pass through the airlight coordinates. We term these lines *haze-lines* to pressure this characteristic (Figs. 1, 2). Pixels along a haze-line come from objects that have similar radiance colours, located over the entire image plane. These objects can be truly are located at different distances from the camera. Since their acquired colour can be modelled by a convex combination of the radiance colour and the airlight colour.

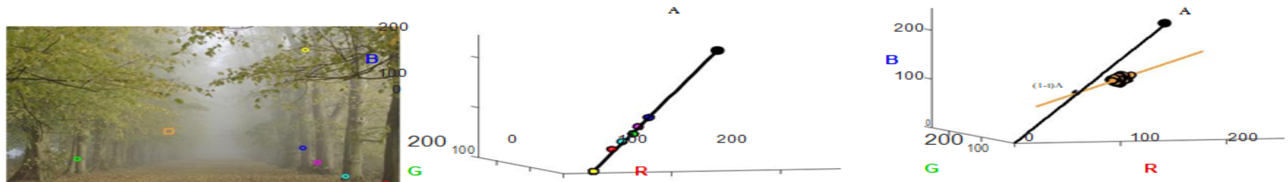

(a) Input hazy image: Forest. Note pixels marked in circles

(b) The circled pixels form a haze-line in RGB colour space

The pixels in the orange square form a colour-line in RGB colour space

The pixels in the orange square form a colour-line in RGB colour space

Fig.2: Haze lines (ours) vs. Colour lines [3]. (a) An input hazy image. Six pixels belonging to related objects in different distances are marked by round colour markers, and a local spot is marked by an orange frame. (b) The colour coordinates of the pixels outline in (a) with round markers are shown in RGB colour space, with a corresponding colour coding. They are distributed over a haze line, as identified by our method. The line passes through the airlight, marked in black. The other end of the line is the haze-free colour of these pixels, not the origin. (c) As opposed to our method, the pixels in the local spot marked by an orange square are distributed along a colour line [3] that intersects the vector from the origin to the airlight.

We suggest an efficient algorithm that is linear in the size of the image. We naturally detect haze-lines and use them to dehaze the image. We also conduct extensive experiments to validate our assumptions and report quantitative and qualitative results on many outdoor images.

II. PREVIOUS WORK

A variety of approaches have been suggested to solve image dehazing. Several methods require additional data to dehaze images, such as multiple images taken under different weather conditions, or two images with different polarization states. Otherwise, the scene geometry is used. Single image dehazing methods assume only the input image is available and depend on image priors.

Haze reduces the contrast in the image, and various methods depend on this observation for restoration. Tan [18] maximizes the contrast per patch, while maintaining a global coherent image. In the amount of haze is estimated from the difference between the RGB channels, which decreases as haze increases.

Some methods use a proceeding on the depth of the image. A smoothness preceding on the airlight is used in, assuming it is smooth except for depth discontinuities. Nishino assume the scene albedo and depth are statistically independent and collectively measure them using priors on both. Manually, either as piece wise constant for urban scenes or smoothly varying for nonurban landscapes.

Several methods assume that transmission and brightness are piece wise constant, and employ a prior on a patch basis.The dark channel priorassumes that within small image patches there will be at least one pixel with a dark colour channel and use this minimal value as an estimate of the present haze. This prior works very well, except in bright areas of the scene where the prior does not hold.

In colour flipsides are matched in RGB space per patch. These flipsides are used to provide a unified approach for previous single image dehazing methods, and a new method is proposed to estimate the transmission in each ellipsoid.

In colour lines are fitted in RGB space per-patch, looking for tiny patches with a constant transmission. This prior is based on the observation that pixels in a haze free image form colour lines in RGB space. These lines pass through the origin and stem from shading variations within objects.

Instead of tiny patches, in [7] the image is segmented to regions with similar distances, and the contrast is stretched within each segment. This may create artefacts at the boundaries between segments.

A. The Prior

While our haze lines might seem similar to [3, 4], they are inherently different. The differences are shown in Fig. 2. In [3], lines are defined by the pixels of small strips in the image plane assuming constant transmission, with intensity differences caused by shading and therefore nearly small (Fig. 2c). This is a *local* phenomena that does not always hold and truly, in [3] care is taken to ensure only strips where the assumption holds are considered. We, on the other hand, look at lines that are formed by separate pixels that are scattered over the entire image. These pixels usually have large intensity differences that are caused by changes in transmission and not local shading effects, as demonstrated in Fig. 2b.

III. PROPOSED WORK

Compared to previous work, we propose an active algorithm that is linear in the size and shape of the image. Haze causes trouble to many computers graphics/vision applications as it reduces the visibility of the scene. So that we are using the EstimateAirlighting.
Estimate airlighting is the basic phenomena of haze.Airlight is increase or decrease the brightness levels in the image. Compared to past,first we are taking the image as per the commands,using the technique as Local Data Set.Compared to previous years, we are clustering the RGB pixel values of each image,using K-means of a maximum of nearly 1000 clusters.
We first present the haze model and then describe how we use non-local haze-lines for image dehazing.

A. 3.1. Haze Model

The common hazy image formation model is [9]:

$$I(x) = t(x) \cdot J(x) + [1 - t(x)] \cdot A\,, \qquad (1)$$

Where$x$ is the pixel coordinates, I is the observed hazy image, and J is the true brightness of the scene point imaged at x. The airlight A is a single colour representing the airlightin image areas where t= 0.
The scene transmission $t(x)$ is distance dependent:

$$t(x) = e^{-\beta d(x)}\,, \qquad (2)$$

Whereβ is the attenuation coefficient of the atmosphere and $d(x)$is the distance of the scene at pixel x. Generally, β iswavelength dependent and therefore t is different per colour channel. This dependency has been assumed negligible in previous single image dehazing methods to reduce the number of unknowns and we follow this assumption. The transmission $t(x)$ acts as a matting coefficient between the scene J and the airlight.
Our procedure is found on the review that the number of different colours in an image is orders of magnitude smaller than the number of pixels.This assumption has been used broadly in the past and is used for saving colour images using indexed colourmaps. We validate and quantify it on the Berkeley Segmentation Dataset (BSDS300). We clustered the RGB pixel values of each image using K-means to a extreme of 500 clusters, and return to every pixel in the image with its corresponding cluster centre. The result is an image with 500 different RGB values at

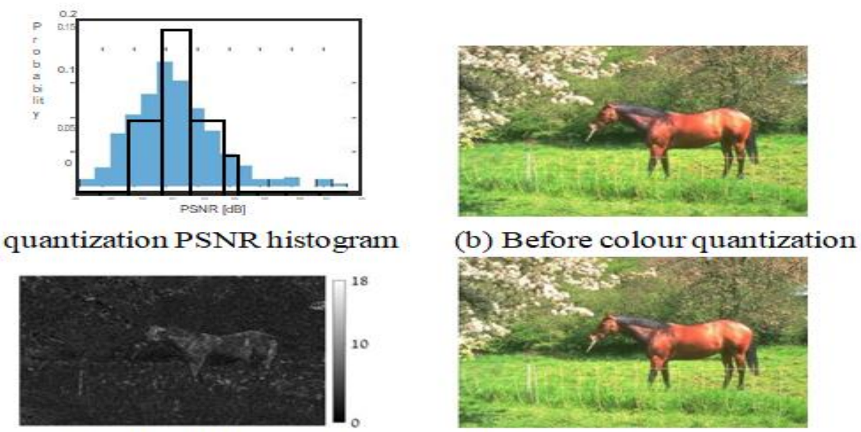

(a) quantization PSNR histogram (b) Before colour quantization
(c) Absolute difference image (d) After colour quantization

Fig3: Prior validation: (a) A PSNR histogram of the quantization errors on the Berkeley Segmentation Dataset (BSDS300): The RGB values of each image were clustered using K-means to 500 clusters and recovered by the cluster centre. The histogram shows the PSNRs measured on the full dataset. (b,d) The image that had the worst PSNR, 36.64dB, before (b) and after (d) colour quantization. (c) Absolute difference image to colour quantized version.

The PSNR of the images develop with the reduced colour set, compared to the original ones, were high and arrange from 36.6dB to 52.6dB. A histogram of the obtained PSNR values is shown in Fig 3, as well as the image that had the worst PSNR, before and after colour quantization.

The survey regarding a small number of different colours holds for haze-free images. In the spirit of haze, object points that belong to the same colour cluster end up with different obtain colours, since they are located in different image areas and thus have different distances from the camera.

This prior is determined in Fig. 1. A haze-free image is clustered using K-means to 500 clusters. The pixels belonging to four of these clusters are decided by different colour markers in Fig. 1a and their RGB coordinates are plot-ted in Fig. 1b, show tight clusters. Note that the clusters include pixels distributed over the entire image that come from objects with different distances from the camera.However, now, colours of pixels that belonged to the same colour cluster are no longer similar. This is depicted in RGB space in Fig. 1d, where the colour coordinates of these pixels are distributed along a haze-line spanned by the original colour and the airlight. The pixels marked by purple circles (originating from the sand patch) are located

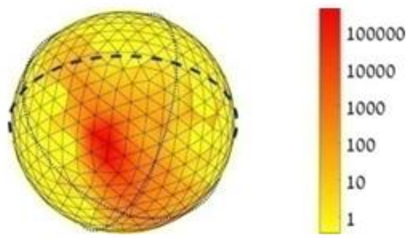

Fig.4: Airlight attract spherical representation. The sphere was sampled uniformly using 500 points. The colour at each point [φ, θ] indicates the number of pixels$x$with these angles whenwriting $I_A(x)$ in spherical coordinates (image size 768×1024).

in the real world, so they are distributed along the haze-line.

Fig. In same distances, so their handling along the haze-line is preferably tight. However, the pixels marked by orange triangles are based at different locations 2 demonstrates the haze-lines prior on a hazy out-door image. Six different pixels recognize by our method as be owned by the same haze line are circled. All of them are on shaded tree trunks and branches, and are likely to have same radiance J. However, their observed intensity I is quite different, as shown in Fig. 2b, where these pixels form a haze-line in RGB space that passes through the airlight.

IV. HAZE REMOVAL

In this method, Our algorithm is at ease of four essential steps: clustering the pixels into haze-lines, estimating an initial transmission map, regularization, and dehazing

A. Finding Haze-Lines:

We measure A using one of the previous methods [2, 5, 18]. Let us define I_A as:

$$ {}_{A}(x) = I(x) - A, $$

i.e., the 3D RGB coordinate system is adapted such that the airlight is at the origin. Following Eq. (1),

$$ {}_{A}(x) = t(x) \cdot [J(x) - A] \ . $$

We express $I_A(x)$ in spherical coordinates:

$$ I_A(x) = [r(x), \theta(x), \varphi(x)] \ . $$

Here r is the distance to the origin (i.e., $I-A$)), θ and φ are the longitude and latitude, respectively.

The colours of the pixels are now represented in a spherical coordinate system around the airlight. Fig. 4 shows the histogram of the Forest image (Fig. 2a) projected onto a sphere. The colour represents the number of pixels pointing at each direction. The equator (φ= 0) is marked by a bold dashed blue line, while the longitudes θ= 0,$\frac{\pi}{2}$ are marked by dotted blue lines. The triangulation is told later. The colour mapping is logarithmic for analogy purposes. The histogram make that the pixels are highly concentrated in terms of their longitude and latitude.

Let us look at Eq. (4). For given values of J and A, scene points at different distances from the camera differ only in the value of t. In the spherical coordinate system Wc .we defined, changes in t affect only $r(x)$ without changing either $\varphi(x)$ or $\theta(x)$. In other words, pixels x and$y$ have same RGB values in the basic haze-free image if their $[\varphi, \theta]$ are same:

$$J(x) \approx J(y) \Rightarrow \{\varphi(x) \approx \varphi(y)\,,\ \theta(x) \approx \theta(y)\},\ \forall t. \quad (6)$$

Therefore, pixels belong to the same haze-line if their $[\varphi(x), \theta(x)]$ values are same. Each point on the spherein Fig. 4 represents a haze-line, in which all the pixels have around the same angles $[\varphi(x), \theta(x)]$. The pixels on each haze-line have same values in the non hazy image J with high probability.

Note that there is inherent uncertainty between colour and haze for colours which are collinear with the airlight:

$$_1 - A = \alpha\,(J_2 - A) \Rightarrow J_1 = (1 - \alpha)A + \alpha J_2\ , (7)$$

Whereα is a scale factor. In this case all single image dehazing methods will correct J_1 and J_2 to the same colour. This is the only case in our method when two colour clusters will be mapped to the same haze-line.

In order to determine which pixels are on the same haze-line, pixels should be grouped according to their angles $[\varphi, \theta]$. A 2-D histogram binning of$\theta$and$\varphi$with uniformedges in the range $[0,2\pi]\times[0, \pi]$ will not generate a uniform sampling of a sphere. Instead, the samples will be denser near the poles [8], since the distance on the sphere is relative to $sin(\theta)$., where each vertex is a sample point. Each vertex corresponds to a haze-line. For clarity of display, the number of samples in Fig. 4 is smaller than the actual number we use. We group the pixels based on their $[\varphi(x), \theta(x)]$ values, according to the closest sample point on the surface. This can be implemented efficiently by building a KD-Tree from the predefined tessellation andquerying the tree for each pixel. This is much faster than running a clustering algorithm such as k-means.

Based on the search described in section 3.2, several hundreds of haze-lines represent an image with a good similarity. Fig. 5a depicts the layout of two different haze-lines in the image plane for the Forest image.

B. *Estimating Initial Transmission:*

For a given haze-line decide by J and A, $r(x)$ depends on object distance:

$$r(x) = t(x)\ J(x) - A\ ,\ 0 \le t(x) \le 1\ . \quad (8)$$

Thus, $t = 1$ corresponds to the largest radial coordinate:

Def J − A . (9)

rmax =

$$r_{max} \overset{Def}{=} J - A\ . \quad (9)$$

Combining Eqs. (8,9) results in an expression for the transmission based on radii in the haze-line

$$t(x) = r(x)/r_{max}\ . \quad (10)$$

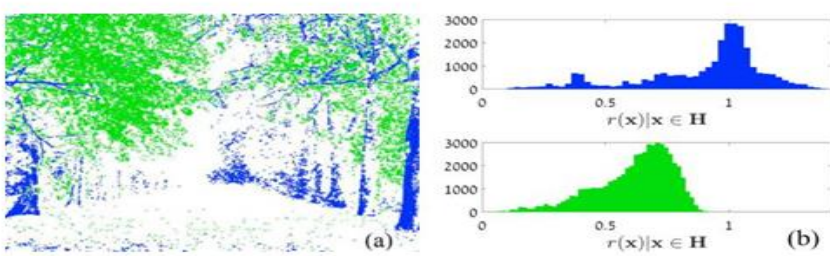

Combining Eqs. (8,9) results in an expression for the transmission based on radii in the haze-line

Figure 5. Distance distribution per haze-line: (a) Pixels belonging to two different haze-lines are represent in green and blue, respectively. (b) A histogram of $r(x)$ within each cluster. The horizontal axis is limited to the range $[0, A]$, as no pixel can have a radius outside that range in this particular image.

Pixel, then $\hat{r}_{max}$ is the maximal radius of that haze-line:

$$\hat{r}_{max}(x) = \max\ \{r(x)\ \}\ , \quad (11)$$

$x \in H$

where the estimation is done per haze-line H. Fig. 5b displays the radii histograms of the two clusters.

$$\tilde{t}(x) = r(x)/\hat{r}_{max}(x) . \quad (12)$$

C. ***Regularization:***

Since the light Jis positive (i.e.,≥ 0), Eq. (1) gives a lower bound on the transmission:

$$t_{LB}(x) = 1 - \min_{c \in \{R,G,B\}} \{I_c(x)/A_c\} . \quad (13)$$

In [5], the transmission measure is based on an eroded version of t_{LB} . We demand this bound on the measured transmission, per pixel:

$$\tilde{t}_{LB}(x) = max\{\tilde{t}(x), t_{LB}(x)\} . \quad (14)$$

$\hat{t}(x)$that is similar to $\tilde{t}_{LB}(x)$and is smooth when the input image is smooth. Mathematically, we minimize the following function w.r.t. $\hat{t}(x)$:

$$\sum_x \frac{\left[\hat{t}(x)-\tilde{t}_{LB}(x)\right]^2}{\sigma^2(x)} + \lambda \sum_x \sum_{y \in N_x} \frac{\left[\hat{t}(x)-\hat{t}(y)\right]^2}{\|I(x) - I(y)\|^2} , \quad (15)$$

Where λ is a parameter that controls trade off between the data and the smoothness terms, N_x denotes the four nearest Neighbours of x in the image plane and $\sigma(x)$ is the standard deviation of t_{LB} , which is calculated per haze-line

D. Algorithm Haze Removal

Step-1:We can read the input image.
Step-2:Convert the input image into Double
Step-3:Convert the Double image into index .
Step-4:Reshaping the given image.
Step-5:After the obtained image, we are subjected to airlighting, where the light increased or decreased.
Step-6:Considered the hazy lines and corrected the hazy lines i.e., line by line.
Step-7:Estimate the initial transmission.
Step-8:Implementing the above process using regularization.
Step-9:Dehazing the obtained image.

$\sigma(x)$plays a expressive role since it allows us to apply our estimate only to pixels where the assumptions hold. When the variance is high, the initial estimation is less reliable. $\sigma(x)$ increases as the number of pixels in a haze line decreases. When the radii distribution in a given haze-line is small, our haze-line assumption does not hold since we do not observe pixels with different amounts of haze. In such cases, $\sigma(x)$ increases as well.

E. Dehazing:

Once $\hat{t}(x)$ is calculated as the minimum ofEq. (15), the dehazed image is calculated using Eq. (1):

$$\hat{J}(x) = \left[I(x) - \left[1-\hat{t}(x)\right]A\right]/\hat{t}(x) . \quad (16)$$

The method is compile in Alg. 1 and establish in Fig. 6. Fig. 6a shows the input hazy image. The final, dehazed image is shown in Fig. 6b. Fig. 6c shows the distance in RGB space of every pixel in the hazy image to the airlight. Note that this space decreases as haze increases. Fig. 6d shows the maximum radii $\hat{r}_{max}(x)$ per haze-line. Observe that Fig. 6d is much brighter than Fig. 6c. Since larger values are represented by brighter colours, this indicates that the distance to the airlight is increased. The pixels with the maximum radius in their haze-line are decided on the hazy image . Therefore mentioned pixels are found in the sky, since the distance to the airlight in RGB space is very short. $\sigma > 2$, since the model expectation do not hold for these haze lines. The aforementioned pixels are form in the sky, since the distance to the airlight in RGB space is very short. Therefore, clustering them according to their angles is not reliable due to noise. In the regularization step this fact is taken into attention through the data term weight 2^1, which is shown in Fig. 6f

$\sigma(x)$

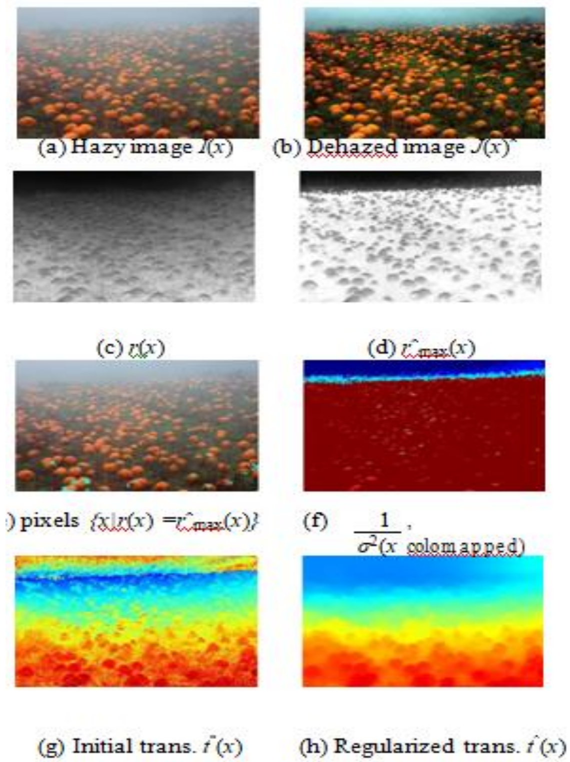

Figure 6. Intermediate and final results of our method: (a) An input hazy image; (b) The output image; (c) The distance $r(x)$ of every pixel of the hazy image to the airlight; (d) the estimated radii (x) calculated according to Eq. (11); (e) The input image isshown, with the pixels x for which $r(x) = \hat{r}_{max}(x)$ marked by cyan circles; (f) The data term confidence in Eq. (15) colourmapped (warm colours show the larger values); (g) The estimated transmission map $\hat{t}(x)$ before the regularization; (h) The final transmission map $\tilde{t}(x)$ after regularization. (g) and (h) are colourmapped.

Mission map after regularization is shown in Fig. 6h. While

$\tilde{}(x)$

Tcontains fine details even in grass areas that are at the

$\hat{}(x)$

Same distance from the camera, t does not exhibit this behaviour. This indicates the regularization is necessary.

V. RESULTS

We calculate our arrangement on a large dataset involves both natural and fabricated images and related our performance to state-of-the-art algorithms.

A. Quantitative results:

A assemble dataset of hazy images of natural scenes was introduced by [3], and is available online. The dataset containsenliven haze free images, fabricated distance maps

Table 1. Comparison of $L1$ errors over fabricated hazy images with various amount of noise. The noise standard deviation is given and the images are scaled to the range [0,1]. The table compares the $L1$errors of the estimated transmission maps (left value) and the dehazed images (right value).

	σ	[5]	[3]	ours
Road1	0	0.097/ 0.051	0.069/ 0.033	0.058/ 0.040
	0.01	0.100/ 0.058	0.068/ 0.038	0.061/ 0.045
	0.025	0.106/ 0.074	0.084/ 0.065	0.072/ 0.064
	0.05	0.136/ 0.107	0.120/ 0.114	0.091/ 0.100
Lawn1	0	0.118/ 0.063	0.077/ 0.035	0.032/ 0.026
	0.01	0.116/ 0.067	0.056/ 0.038	0.032/ 0.032
	0.025	0.109/ 0.077	0.056/ 0.065	0.052/ 0.056
	0.05	0.115/ 0.102	0.114/ 0.121	0.099/ 0.107
Mansion	0	0.074/ 0.043	0.042/ 0.022	0.080/ 0.049
	0.01	0.067/ 0.040	0.048/ 0.030	0.088/ 0.056
	0.025	0.057/ 0.044	0.065/ 0.051	0.104/ 0.072
	0.05	0.083/ 0.075	0.081/ 0.080	0.116/ 0.095
Church	0	0.07/ 0.048	0.039/ 0.025	0.047/ 0.032
	0.01	0.067/ 0.050	0.053/ 0.043	0.049/ 0.041
	0.025	0.058/ 0.059	0.089/ 0.081	0.047/ 0.057
	0.05	0.087/ 0.121	0.121/ 0.136	0.043/ 0.092
Raindeer	0	0.127/ 0.068	0.066/ 0.034	0.089/ 0.045
	0.01	0.119/ 0.066	0.077/ 0.042	0.093/ 0.049
	0.025	0.109/ 0.067	0.084/ 0.054	0.104/ 0.063
	0.05	0.117/ 0.085	0.106/ 0.083	0.131/ 0.092

And corresponding simulated haze images. An identically distributed zero mean Gaussian noise with three different noise level: σ_n= 0.01,0.025,0.05 was added to these images (with image intensity scaled to [0,1]). Table 1 summarizes the L_1 err`ors on non sky pixels (same metric used in [3]) of the transmission maps and the dehazed images. Our method is compared to the method of [3] and an implementation of [5] by [3]. For five images out of this dataset, results of both clear and noisy images are provided by [3][1].

Our method outperforms previous methods in most cases, and handles the noise well. As expected, our performance degrades when the noise variance increases. How-ever, our method maintains its ranking, with respect to other methods, regardless of the amount of noise. This shows that our algorithm is quite strong to noise, despite being pixel-based.

B. Qualitative results

Figs. 7 and 8 compare our results to state-of-the-art single image dehazing methods. As previously notedby the image after haze removal might look dim, since the scene radiance is usually not as bright as the airlight.

A complete summary of results and more is available on the project's website.

hazy image: House He *et al*. [5] Gibson and Nguyen [4] Nishino *et al*. [12] Fattal [3] Ours

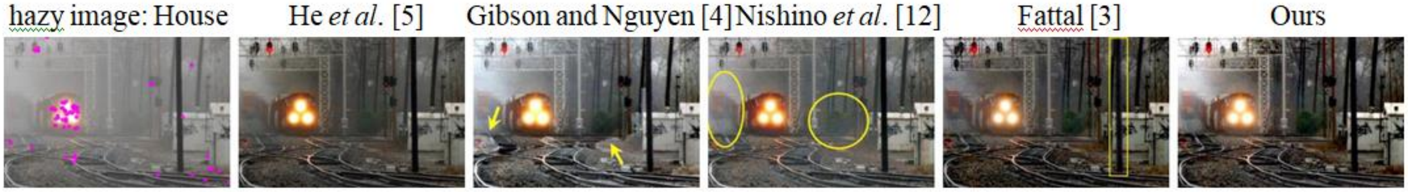

hazy image: Train He *et al*. [5] Luzon´-Gonzalez´ *et al*. [7] Ancuti and Ancuti [1] Fattal [3]

hazy image: Cityscape He *et al*. [5] Gibson and Nguyen [4] Tang *et al*. [19] Fattal [3] Ours

Fig.7: Comparison on natural images: [Left] Input with pixels that set the maximum radius in their haze-line circled in pink. [Right] Ourresult. Middle columns display results by several methods, since each paper reports results on a different set of images.

Top to bottom: hazy image: Forest He *et al*. [5] results Fattal [3] results our results

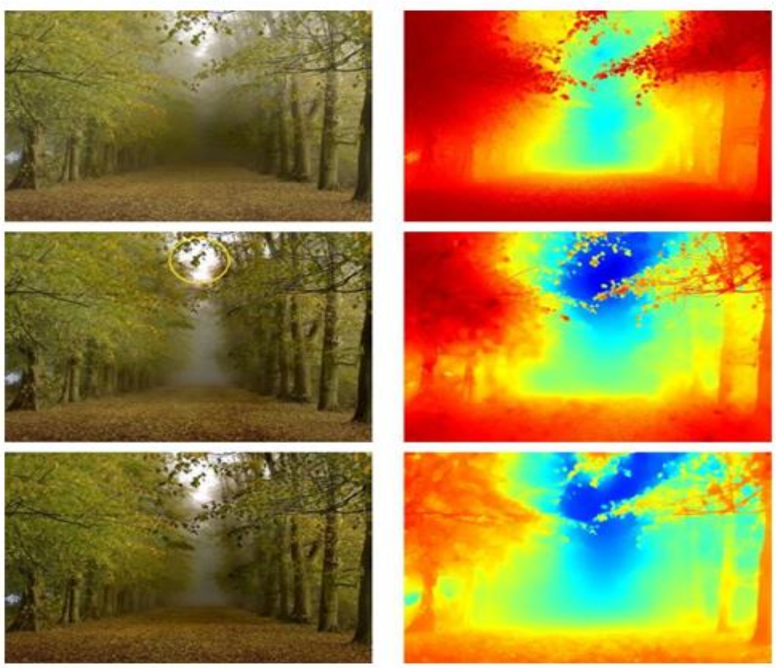

Fig. 8: Comparison of transmission maps and dehazed images

The method of [1] split haze in the results, as seen in the areas circled in yellow in Fig.7. In the result of [7] there are artefacts in the boundary between portions (pointed by arrows). The method of [12] tends to overinfuse (e.g., House). The methods of [5, 19] assembled excellent results in common but lack some micro contrast when compared to [3] and to ours. This is clear in the zoomed in buildings shown in Cityscape results, where in our result and in [3] the windows are sharper than in [5, 19] (best viewed on a monitor). The result of [4] was not enlarged as it has a low resolution. Results of [3] are sometimes sniped, e.g., the blades in House and in the sky in Forest.

Our expectation about having a haze-free pixel in each haze-line does not hold in Cityscape, as marked by several hazy pixels that set a maximum radius, e.g. the red buildings. Against that, the transmission in those areas is estimated correctly due to the regularization that cultivates the depth information spatially from the other haze-lines.

Fig. 8 compares both the transmission maps and the de-hazed images. It shows our method is comparable to other methods, and in conclusive cases works improved. For example, the two rows of trees are well divided in our result when compared to [5].

The main advantage of the global approach is the ability to conduct well with fast variations in depth, when the details are smaller than the patch size. Fig. 9 shows an extended

Fig.9: (a) Hazy input. (b) The result of [5]. (c) The result of

(d) Our result. Note the artefacts around the leaves and the branch at (c). This is a result of the patch-based method. While is also a patch-based and does not exhibit these artefacts, this method underestimates the haze in this image, so the depth gap is not pronounced. Note the missing details in the tree trunk of (b) compared to (c) and (d).

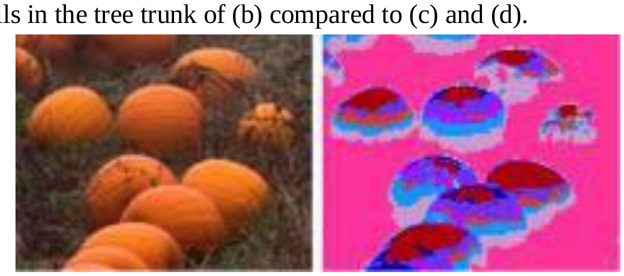

Fig.10: Colour Clustering: Left: a crop of Fig. 6a). Right: a cluster map eachcolourrepresents a different haze line. The steady tone change of the pumpkins is preserved in the clustering.

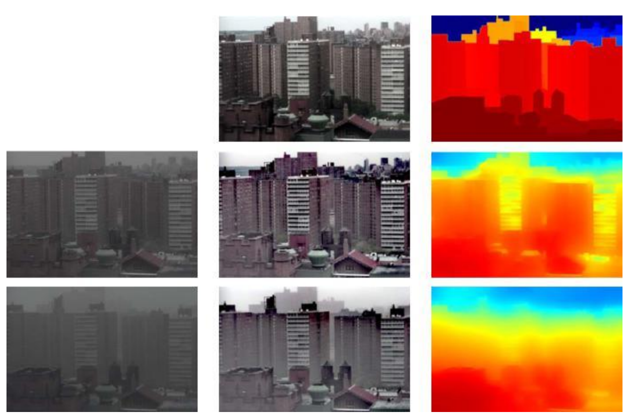

Fig.11: Top row: clear day image and ground truth depth of the scene. Two bottom rows, from left to right: an image taken in bad climate conditions, our result and the transmission map.Portion of an image, where clear artefacts are visible in the result of [3], around the leaves and at the boundary between the trunk and the background. A patch-based method is less likely to approximate the distance of such scenes accurately. The result of [5] does not fair these artefacts in Fig. 9, since the dehazing is less adequate in this image and the details are less clear (e.g, the circled trunk). This phenomena is also visible in Fig. 7 in the dehazed Cityscape image of [4], where glory between the trees in the foreground and the background is visible, and also in the train output of [3] around the pillar (marked by a yellow square).

Using a fixed tessellation of the unit sphere might raise a concern that fine tones will not be distinguished. Fig. 10 demonstrates this is not the case. The pumpkins (a crop of Fig. 6a) are lit from above, and therefore are shining at the top and slowly become darker towards the ground

(Fig. 10 left). Fig. 10 right depicts the cluster map - each colour symbolizes a different haze-line. The gradual tone change is evident in the cluster map.

The climate and Illumination Database (WILD) [10] carry multiple images of the same scene and the ground truth depth. Fig. 11 shows on the top row a clear day image of the scene as well as the depth. Below are images taken under bad climate conditions and our results. The image at the middle row was taken in light rain and mist, and our method restores the visibility while estimating a rough depth map. The image at the bottom left was taken down heavy fog and limited visibility.

C. Complexity analysis

Our method is definite in N, the number of pixels in the image, and therefore fast. The clustering is done using a nearest neighbour search on a KD-Tree with a fixed number of points. Estimating the radius within each cluster is linear in N . Therefore, the initial radius estimation is $O(N)$. Seeking the minimum of Eq. (15) requires explanation of a sparse definite system, which is also $O(N)$. Restoring the dehazed image from the transmission map is $O(N)$ as well.

VI. CONCLUSION

We have introduced a technique to removal of the foggy noise in outdoor images is based on estimate airlighting. Compared to existing work, we proposed an efficient algorithm that is linear in size and shape of the image. Due to the haze, small particles in the air that scatter the light in the atmosphere so, the outdoor images often suffer from low contrast and finite visibility So that, the problem was cleared by using function as estimate airlighting. In this airlighting, several types of sub functions are used to remove unwanted noise in outdoor images and gives clear visibility of an image.

VII. REFERENCES

[1]. C. O. Ancuti and C. Ancuti. Single image dehazing by multi-scale fusion. IEEE Trans. on Image Processing, 22(8):3271– 3282, 2013.
[2]. R. Fattal. Single image dehazing. ACM Trans. Graph., 27(3):72, 2008.
[3]. R. Fattal. Dehazing using color-lines. ACM Trans. Graph., 34(1):13, 2014.
[4]. K. B. Gibson and T. Q. Nguyen. An analysis of single image defogging methods using a color ellipsoid framework. EURASIP Journal on Image and Video Processing, 2013(1), 2013.
[5]. K. He, J. Sun, and X. Tang. Single image haze removal using dark channel prior. In Proc. IEEE CVPR, 2009.
[6]. J. Kopf, B. Neubert, B. Chen, M. Cohen, D. CohenOr, O. Deussen, M. Uyttendaele, and D. Lischinski. Deep photo: Model based photograph enhancement and viewing. ACM Trans. Graph., 27(5):116, 2008.
[7]. R. Luzon´-Gonzalez,´ J. L. Nieves, and J. Romero. Recovering of weather degraded images based on RGB response ratio constancy. Appl. Opt., 2014.
[8]. G. Marsaglia. Choosing a point from the surface of a sphere. Ann. Math. Statist., 43(2):645–646, 04 1972.
[9]. W. E. K. Middleton. Vision through the atmosphere. Toronto: University of Toronto Press, 1952.
[10]. S. Narasimhan, C. Wang, and S. Nayar. All the Images of an Outdoor Scene. In European Conference on Computer Vision (ECCV), volume III, pages 148–162, May 2002.
[11]. S. G. Narasimhan and S. K. Nayar. Chromatic framework for vision in bad weather. In Proc. IEEE CVPR, 2000.
[12]. K. Nishino, L. Kratz, and S. Lombardi. Bayesian defogging. Int. Journal of Computer Vision (IJCV), 98(3):263– 278, 2012.
[13]. I. Omer and M. Werman. Color lines: Image specific color representation. In Proc. IEEE CVPR, 2004.
[14]. M. T. Orchard and C. A. Bouman. Color quantization of images. Signal Processing, IEEE Transactions on, 39(12):2677–2690, 1991.
[15]. D. Park, D. K. Han, C. Jeon, and H. Ko. Fast single image de-hazing using characteristics of RGB channel of foggy image. IEICE Trans. on Information and Systems, 96(8):1793–1799, 2013.
[16]. Y. Y. Schechner, S. G. Narasimhan, and S. K. Nayar. Instant dehazing of images using polarization. In Proc. IEEE CVPR, 2001.
[17]. M. Sulami, I. Ge5ltzer, R. Fattal, and M. Werman. Automatic recovery of the atmospheric light in hazy images. In Proc. IEEE ICCP, 2014.
[18]. R. Tan. Visibility in bad weather from a single image. In Proc. IEEE CVPR, 2008.
[19]. K. Tang, J. Yang, and J. Wang. Investigating haze-relevant features in a learning framework for image dehazing. In Proc. IEEE CVPR, 2014.
[20]. J.-P. Tarel and N. Hautiere. Fast visibility restoration from a single color or gray level image. In Computer Vision, 2009 IEEE 12th International Conference on, pages 2201–2208, Sept 2009.

[21]. Q. Zhu, J. Mai, and L. Shao. Single image dehazing using color attenuation prior. In proc.British Machine Vision Conference (BMVC), 2014

Ms. K. Hema Maline working as a Assistant Professorof Electronics and Communication Engineering in Swarnandhra College of Engineering and Technology, Narasapur,Andhra Pradesh.

Ms.G.Aparanjita Pursuing B.Tech in Swarnandhra College of Engineering and Technology,Narasapur,Andhra Pradesh.

Ms.D.SriLalitha Pursuing B.Tech in Swarnandhra College of Engineering and Technology,Narasapur,Andhra Pradesh.

Mr.CH.L V D Vara Prasad Pursuing B.Tech in Swarnandhra College of Engineering and Technology,Narasapur,Andhra Pradesh.

Mr.M.T S Chandu Pursuing B.Tech in Swarnandhra College of Engineering and Technology,Narasapur,Andhra Pradesh.